

# Collision Avoidance in Human-Robot Interaction Using Kinect Vision System Combined With Robot's Model and Data

Hugo Nascimento<sup>1,2</sup>, Martin Mujica<sup>2</sup> and Mourad Benoussaad<sup>2</sup>

**Abstract**—Human-Robot Interaction (HRI) is a largely addressed subject today. Collision avoidance is one of main strategies that allow space sharing and interaction without contact between human and robot. It is thus usual to use a 3D depth camera sensor which may involves issues related to occluded robot in camera view. While several works overcame this issue by applying *infinite depth* principle or increasing the number of cameras, we developed in the current work a new and an original approach based on the combination of a 3D depth sensor (Microsoft® Kinect V2) and the proprioceptive robot position sensors. This method uses a principle of limited *safety contour* around the obstacle to dynamically estimate the robot-obstacle distance, and then generate the repulsive force that controls the robot. For validation, our approach is applied in real time to avoid collision between dynamical obstacles (humans or objects) and the end-effector of a real 7-dof Kuka LBR iiwa collaborative robot.

Several strategies based on *distancing* and its combination with *dodging* were tested. Results have shown a reactive and efficient collision avoidance, by ensuring a minimum obstacle-robot distance (of  $\approx 240mm$ ), even when the robot is in an occluded zone in the Kinect camera view.

## I. INTRODUCTION

Humans and robots working together or sharing the same space could reach an extraordinary level of performance if they combine the human decision-making capabilities and the robot's efficiency [1], [2], however, this collaboration has to be safe for humans beings.

Human-Robot Interaction (HRI) is a novel and promising trend in robotics research, since an increasing number of works were addressed in this field [3], [4]. One aspect of HRI is physical Human-Robot Interaction (pHRI), which deals with the collision detection [5] and a continuous physical interaction [6]. Another aspect of HRI is collision avoidance, where the robot adapts its predefined trajectory to avoid collision with dynamic obstacles (humans or objects) [7], [8], [9], [10]. Collision Avoidance using human wearable sensors were explored in [10]. However, this solution presents the equipment complexity and thus limits the interacting people number. Furthermore, collision avoidance based on 3D depth camera (Microsoft Kinect) were explored [7], [8], [9]. In these works, it is usual to retract the robot from the scene to detect and track only obstacles. Authors in [7] explored the depth space to compute distances between the robot and dynamic obstacles in real-time and then, the

robot was controlled using virtual repulsive forces principle. The obstacle-robot distance estimation methods were more deeply explored in [11] by developing an improved and faster method for a real time application.

However, using Kinect implies robot occlusion issues when the obstacle is between the robot and the camera. To overcome these issues, different approaches were explored. One approach used multiple Kinects to increase the workspace representation. Authors of [8], [9] used two Kinects in a similar way, however authors in [9] applied a collision avoidance of a 6-dof robot manipulator, while keeping its task by including Cartesian constraints. Furthermore, the use of multiple Kinects, increases the calibration complexity between them and the computational cost.

Other approach using one Kinect only, considered the obstacle with an *infinite depth*, called a *gray area* [6], [7], [11]. Although this approach highlighted efficient results and prioritized the human safety, it presents a too conservative behavior. For instance, when the obstacle is placed between the robot and the camera, it will be considered close to the robot even when it is far from it in the depth axis, and thus it can not deal with the case of obstacles that hide completely the robot from the camera's view. Moreover, all these previous works that used Kinect to extract the robot pose had to manage the unavoidable noise that comes from the vision system.

In the current work, we explore a new approach for collision avoidance between dynamic obstacles and the robot's End-Effector (*E-E*), which can be completely hidden by obstacles. Our method differs from previous works, for dealing with this case, by merging the robot kinematic model and its proprioceptive data in the 3D depth data of the environment. Moreover, as an alternative to *infinite depth* strategy [7], [11] and its above-mentioned issues, we applied a limited *safety contour* around the obstacle to avoid unnecessary robot movement and deal with the case of hidden robot's *E-E*.

In the next Section an overview of the system and the description of the materials are presented. Then our collision avoidance approach is described in Section III. Results are presented and discussed in Section IV, then a conclusion and the perspectives of this work are summarized in Section V.

## II. MATERIALS AND SYSTEM OVERVIEW

This section describes the whole system overview (hardware/software) and introduces the Kinect's depth principle and the collaborative robot used.

<sup>1</sup> Hugo N. Author is with Polytechnic school, Automation and control department, University of Pernambuco, R. Benfica, 455 - Madalena, Recife - PE, 50720-001. Brazil; hugonascimentoal@gmail.com

<sup>2</sup> Martin M. and Mourad B. authors are with LGP-ENIT, University of Toulouse, Tarbes, France; {martin.mujica, mourad.benoussaad}@enit.fr

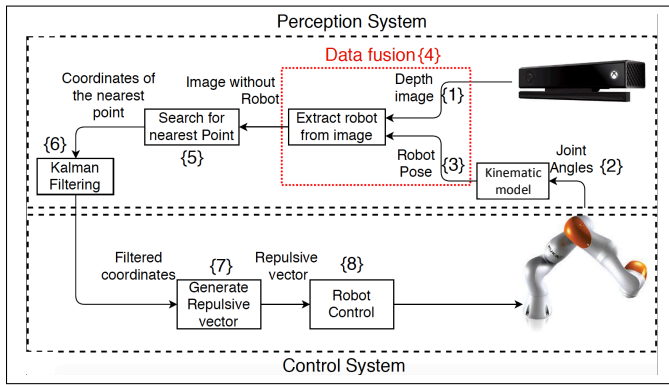


Fig. 1: Collision avoidance system overview.

### A. Whole system overview

The whole system overview is illustrated by Fig. 1. It includes a *Perception system* and a *Control system* which works in a real-time closed-loop. The *perception* combines vision acquisition through Kinect {1} and the robot pose using joint angles {2} along with its kinematic model {3}. This robot pose is projected in the depth space using data fusion {4}, which allow removing the robot from the image. Then the obstacle's nearest point to the robot in a *supervised zone* is detected {5} and its coordinates are filtered using a Kalman filter {6} to handle the noise related to the depth image. The distance between the obstacle's nearest point and the robot's *E-E* is used in the control part, by generating a repulsive vector {7} to control and adapt the robot posture {8} in order to avoid collisions with dynamic obstacles.

### B. Kinect and depth space representation

The used Kinect V2 is placed in the range between 0.5m and 4.5m from robot, where the maximum data rate is about 30Hz. From depth image (grayscale image of  $512 \times 424$  resolution) [12], (1) is used to get a point in the Kinect's frame from its pixel address on the depth image.

$$\begin{cases} x_r = (x_i - c_x)d_p/f_x \\ y_r = (c_y - y_i)d_p/f_y \\ z_r = d_p \end{cases} \quad (1)$$

Where  $c_x$  and  $c_y$  are the coordinates of a so-called generic Cartesian point in  $X$  and  $Y$  axis,  $f_x$  and  $f_y$  are the focal lengths along  $X$  and  $Y$  axis and  $d_p$  is the depth of the pixel.  $(x_i, y_i)$  are coordinates of the pixel on the image and  $(x_r, y_r, z_r)$  represents real point coordinates in the Kinect frame.

### C. Collaborative robot and practical aspects

A 7-dof redundant manipulator (Kuka LBR Iiwa R820 collaborative robot) has been used. To control the robot and get its proprioceptive data using an external system in real time, *Fast Robot Interface* (FRI) software option was adapted and used [13]. The FRI control is based on an *overlay* principle which consists of superposing a control input, derived from the external system (with our method), and a local robot control law.

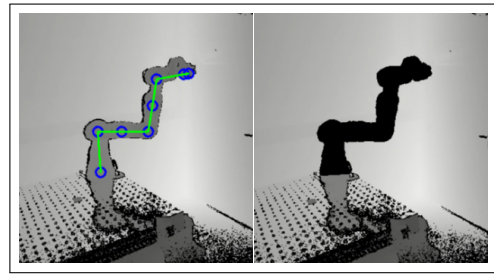


Fig. 2: Robot depth image with its skeleton (left) and after its extraction from image (right).

## III. COLLISION AVOIDANCE STRATEGIES

This section describes the used methodology. It starts from the perception of the robot and environment until the control law, following steps presented in Fig. 1.

### A. Robot Kinematic model

Kinematic model of our robot was established from [14]. It is used to describe and update the robot's pose (a skeleton of Fig. 2-left) from the measured robot's joint angles (FRI §II-C). Hence, the robot pose is updated in real-time, even when the Kinect camera does not see it (robot in occluded zone).

### B. Depth image and robot intrinsic data fusion

To handle the obstacle-robot collision, it is necessary to know what points correspond to the robot in order to consider all the other points as corresponding to the environment (possible obstacles). Indeed, if a point of the robot is not identified and removed from image, it can be considered as a possible obstacle, particularly if it is in a *supervised zone*. Therefore, with the kinematic model and joint angles, a robot skeleton was implemented and updated, as a real robot, on the 3D depth image, which makes possible the robot identification. This skeleton augmented with a predefined 3D robot form is then used to remove it from the image and obtaining a depth image without the robot. These steps are illustrated by Fig. 2, where the left side shows the robot skeleton added to the depth image, and the right side shows the depth image with the robot removed. However, these steps are possible if a robot data fusion is done between a depth image space and its intrinsic data. This data fusion consists of linking the robot skeleton, updated from its intrinsic data and model, with points of robot (or a visible part) in the image. Hence, a precise representation between Kinect frame and the robot frame is required. For that, an offline calibration procedure was implemented using the three known points technique [15].

### C. Nearest point: searching and filtering

A *supervised zone*, where an obstacle is searched, was chosen and implemented as a spherical shape, which center is the robot's *E-E*, as illustrated by Fig. 3. The method searches in the depth image inside this sphere for the obstacle nearest point from the sphere center (Fig. 3). The collision

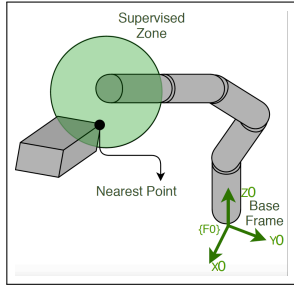


Fig. 3: *Supervised zone* and its nearest point.

avoidance strategy is based on the position of this point with respect to (w.r.t.) the robot's *E-E*, which makes its estimation quality very important for robot control and smooth motion. Therefore, to ensure this estimation quality, this point's position was filtered with a Kalman filter since it is known to be fast, optimal and lite [16]. To apply this Kalman filter, a constant velocity model [9] of point motion was adopted and implemented.

#### D. Distance evaluation

Our approach of collision avoidance is based on robot-obstacle distance estimation. It is calculated using Euclidean distance  $d_1$  between obstacle nearest point  $P_o$  (see §III-C) and a robot *E-E* point  $P_e$  (see §III-B). To consider the occlusion risk of the robot by the obstacle, we distinguish two use cases (Fig. 4):

**Case 1: No occlusion risk.** When the obstacle has a greater depth than the robot *E-E* ( $z_1 > z_e$ ) in the camera point of view (Fig. 4-Case 1), the distance  $d_1$  is used in the collision avoidance method.

**Case 2: risk of occlusion.** When the obstacle has a lower depth than the robot *E-E* ( $z_e > z_1$ ), there is a risk of occlusion. In this case, we do not consider *infinite depth* strategy for the obstacle as in [7]. Instead, we used a *safety contour* around the point that we are dealing with (visible nearest point), as shown by Fig. 4-Case 2. Hence, we limit the influence of obstacle on the robot, even keeping a safety distance:

$$d_2 = d_1 - R \quad (2)$$

Where  $d_1$  is calculated as mentioned before and  $R$  is the radius of the safety contour. The choice of its value is based on the rough estimation of the obstacle (or the human hand) size, by considering the longest distance between two points of it. Hence, In case 2, it is the safety distance  $d_2$  which is used in collision avoidance method.

#### E. Potential field

To ensure collision avoidance of the robot with dynamic obstacles, the potential field method was applied [17]. In this method, the dynamic obstacle creates a repulsive force which is used here through two strategies: *Distancing* and *Dodging*. These strategies are based on intuitive human collision avoidance (example of bullfight).

**Distancing strategy:** It is an intuitive method that consists of distancing the robot from the obstacle in the same line than

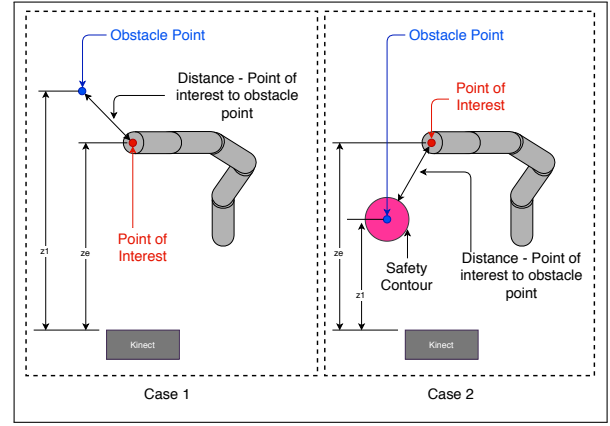


Fig. 4: Methods for distance evaluation (two cases). Case 1: no risk of occlusion. Case 2: with risk of occlusion

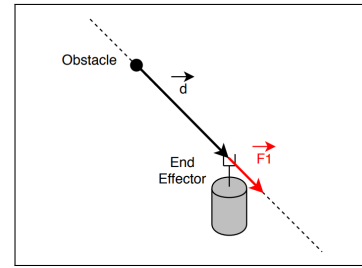


Fig. 5: Distancing strategy principle.

vector  $\vec{d}$ , which links the obstacle to robot *E-E*, by applying a repulsive force as illustrated by Fig. 5.

The model of repulsive force is defined as in [7]:

$$\vec{F}_1 = \frac{\vec{d}}{\|\vec{d}\|} V \quad (3)$$

Where  $V$  is the force intensity defined as an inverted sigmoid function of the distance between obstacle and robot's *E-E*:

$$V = \frac{V_{max}}{1 + e^{(\|\vec{d}\| (2/\rho) - 1)\alpha}} \quad (4)$$

$V_{max}$  is the maximal force intensity,  $\alpha$  a shape factor and  $\rho$  a parameter related to the *supervised zone* size [7]. Therefore, the repulsive force intensity  $V$  will be  $V_{max}$  when robot-obstacle distance vanish, and should approach zero when the distance reaches *supervised zone* limits, since the force is not defined beyond.

**Dodging strategy:** In this technique, instead of moving like the obstacle and in the same direction, the end-effector dodges the obstacle by moving in another direction thanks to the Cartesian force  $\vec{F}_2$  (see Fig. 6a). In the current work, this direction is chosen to be on the plan  $(X_e, Y_e)$  (in yellow) of the robot's *E-E* frame (Fig. 6a), where  $Z_e$  is the axis of the last joint robot. Therefore, the force  $\vec{F}_2$  is given by the equation:

$$\vec{F}_2 = \frac{\overrightarrow{Proj}(d)_{(X_e, Y_e)}}{\|\overrightarrow{Proj}(d)_{(X_e, Y_e)}\|} V \quad (5)$$

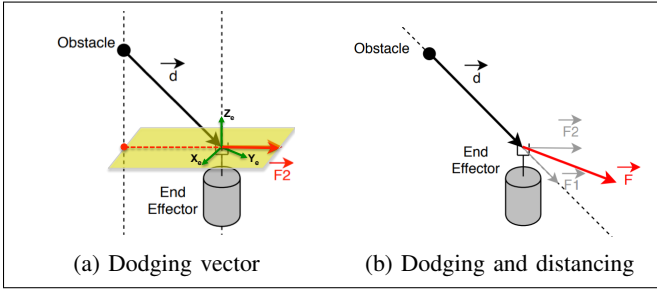


Fig. 6: Dodging and distancing combination strategy.

Where  $\overrightarrow{Proj}(d)_{(X_e, Y_e)}$  is the projection of vector  $\vec{d}$  in the plan  $(X_e, Y_e)$  and  $V$  is the repulsive force intensity defined by (4). A generalization of this *dodging* strategy is made here in practice. In fact, a Cartesian force applied on the robot's *E-E* is actually  $\vec{F}$ , which is a linear combination of *distancing* vector  $\vec{F}_1$  and *dodging* vector  $\vec{F}_2$ , as illustrated by Fig. 6b and described by (6):

$$\vec{F} = \beta_1 \vec{F}_1 + \beta_2 \vec{F}_2 \quad (6)$$

Where  $\beta_1$  and  $\beta_2$  are parameters to adjust to give the robot more *distancing* or more *dodging* behavior, as required by the application.

For both strategies, the calculated repulsive force was applied as a wrench (Cartesian forces) at the robot *E-E*. In Kuka LBR iiwa, this wrench is superposed to an existing local control law, by using FRI software tool (§II-C).

#### IV. EXPERIMENTAL RESULTS AND DISCUSSION

In this section, experimental tests and results of the collision avoidance strategies are presented and discussed to analyze and assess our proposed method. The experimental setup includes a 7-dof Kuka LBR Iiwa with its controller, a Kinect V2 and an external computer (*Intel Core i7; 2.5Ghz × 8; 16 GiB Memory; NVIDIA Quadro K2100M as graphics; Ubuntu 18.04 as OS*). Kinect was placed on a rigid support at 2.346m from the robot, precisely in the robot coordinate (140mm, 431mm, 2302mm).

Parameters of our methods and strategies defined above can be adjusted for each application purpose. However, they were adjusted in the current experiment as follows. The *supervised zone* diameter value is fixed to 1.1m and safety contour radius  $R = 150\text{mm}$  (based on the obstacle's size knowledge); Parameters of force intensity function of (4) are  $\alpha = 5.0$ ,  $\rho = 0.425$  and  $V_{max} = 45.0\text{N}$ ; Parameters of forces linear combination of (6) are  $\beta_1 = 1.8$  and  $\beta_2 = 1.0$ . The way to adjust  $\beta_1$  and  $\beta_2$  can be explored in future works, meanwhile it is experimentally adjusted and fixed in the current work to test the method.

The background task (robot task when there is no obstacle) is to keep its initial configuration with a compliant Cartesian behavior in translation (*i.e.* with a virtual Cartesian mass-spring-damper system) using an impedance controller of Kuka LBR iiwa [18]. For the three axis, the stiffness was fixed to 300N/m and the damping ratio to 1. Then, our

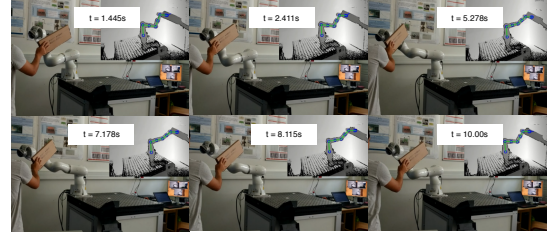


Fig. 7: Images sequence of collision avoidance test with the robot in an occluded zone.

collision avoidance strategies and robot control overlay (*i.e.* external control superposed to local robot control) were applied at a wrench level through FRI command mode in real time.

In the following experiments, *distancing* strategy is applied when robot is in an occluded zone to highlight our method robustness. Then a test with multiple and repetitive collision avoidance is proposed to show results reproducibility and finally, the *dodging* strategy is tested and analyzed. Results are then discussed where *dodging* and *distancing* strategies are compared.

##### A. Collision avoidance with the robot in an occluded zone

In the current test, a Cardboard box (dynamic obstacle) was used to move toward the robot *E-E*, while keeping it in an occluded zone. Hence, the robot's *E-E* remains behind the obstacle w.r.t. the Kinect viewpoint. Fig. 7 shows an images sequence of this experiment, where a RGB image is the main picture and a grayscale image (Kinect viewpoint) with a robot skeleton is at the top-right. We can notice in the grayscale images that the robot is hidden behind the cardboard box w.r.t. Kinect. Results of this test, presented in Fig. 8, show the evolution of the obstacle-robot's *E-E* distance while the robot is in an occluded zone. It highlights that this distance never cross the limit of 150mm (red line), which corresponds to safety contour radius ( $R$ ).

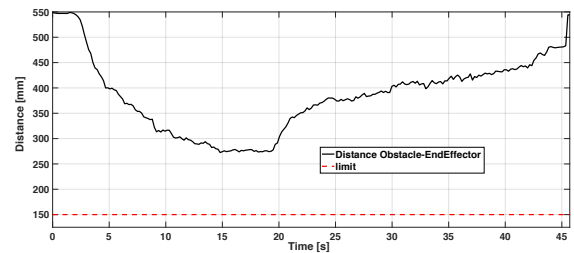


Fig. 8: Obstacle-Robot *E-E* distance evolution during the test with the robot in an occluded zone and distance limit (red).

##### B. Multiple collision avoidance

As mentioned before, the current test purpose is to explore reproducibility of our solution. It was realized in the same conditions and with the same strategy (*distancing*) than the previous test. Fig. 9 shows the evolution of the obstacle-Robot's *E-E* distance for multiple collision attempts between



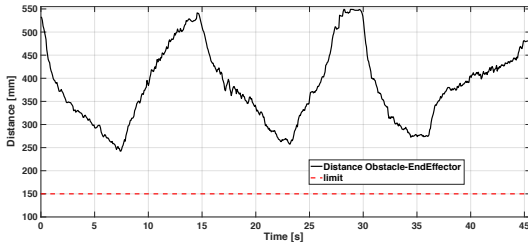


Fig. 9: Evolution of obstacle-Robot  $E-E$  distance during multiple collision attempts and distance limit (red).

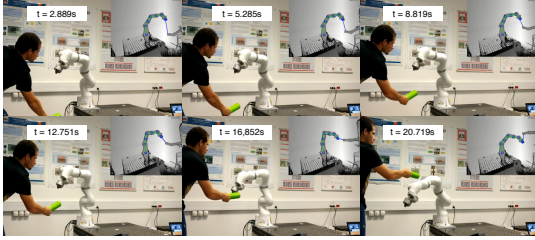


Fig. 10: Images sequence of *dodging* strategy test.

them. Results highlight that our collision avoidance strategy, by controlling the robot, keep always enough distance from the limit of  $150mm$  (red line) even with multiple collision attempts. The minimum distance was at time  $7.2s$  and had a value of  $242mm$ .

### C. Dodging Strategy

In the current test, the obstacle was moved vertically ( $Z$  axis) from the bottom in direction of robot  $E-E$  in order to analyze the *dodging* strategy, as illustrated by the images sequence of Fig. 10. In the grayscale part of each image (top-right), the blue line, representing the obstacle-robot's  $E-E$  distance, is firstly almost vertical (at  $t \approx 2.89s$ ), then it tends to become horizontal (at  $t \approx 16.85s$ ), which shows that robot dodges the obstacle movement by taking a different direction. To analyze more deeply these results, Fig. 11 highlights the evolution of  $Y$  and  $Z$  coordinates of the robot's  $E-E$  and the obstacle in the robot base frame  $\{F0\}$  (see Fig. 3). Obstacle  $Z$  coordinate increases (vertical movement) until crossing those of robot  $E-E$  (at  $t \approx 16s$ ), while  $Y$  coordinates of both are close at the beginning and diverge thereafter, which is typical of dodging behavior. We can also notice a small  $Z$  coordinate variation of robot  $E-E$ , related to the *distancing* vector  $\vec{F1}$  in the *dodging and distancing combination* strategy (6). The  $X$  coordinates are not presented since they are not very relevant for this movement which occurs basically on the  $Y$  and  $Z$  directions. Despite crossing of the different coordinates, a certain distance between obstacle and robot  $E-E$  is respected, avoiding thus the collision, as illustrated by Fig. 12. We can notice that the instant of minimum distance corresponds almost to the one of  $Z$ -coordinates crossing (between the robot's  $E-E$  and the obstacle).

### D. Discussions

Overall, results highlight robot's capabilities to avoid collisions with dynamic obstacles, even when it is in an

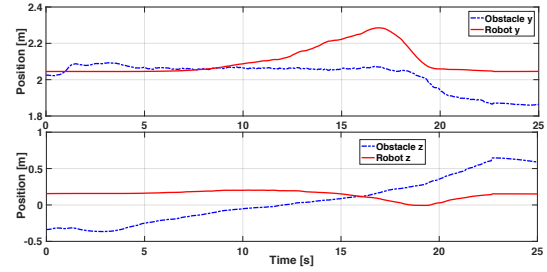


Fig. 11:  $Y$  and  $Z$  coordinates of the obstacle and the robot  $E-E$ .

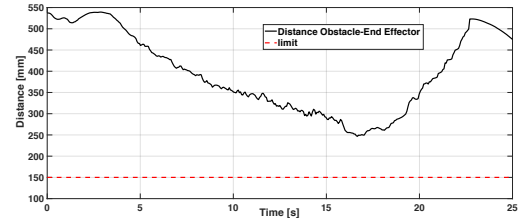


Fig. 12: Obstacle-Robot  $E-E$  distance evolution during the *dodging* strategy test.

occluded zone w.r.t. Kinect. Indeed, the proprioceptive robot data (joint angles), provided by *FRI monitor mode* in real time, combined with the robot kinematic model allow robot posture estimation with a small uncertainty even without being seen by Kinect. In this case, a safety contour, based on the nearest point detected, was defined (Fig. 4-Case 2) since the real obstacle nearest point may not be visible for the camera either. This allows a less conservative safety strategy than in [7], by assuming roughly the obstacle size knowledge and thus fixing the contour radius  $R$ . As a perspective, this contour radius size can be adapted online by considering also the obstacle speed estimation in the adaptive law. In addition, the robot posture estimation is more stable and does not suffer from the noise that can come from the vision system. However, since the collision avoidance strategy is based on the obstacle-robot distance, vision-based estimation of the obstacle position still presents noise issues. Hence, filtering of these data was required, and done in the current work.

*Distancing* strategy presented satisfactory and efficient results, however the *dodging* strategy was conceived to overcome robot space reachability problems, which would appear using *distancing* strategy. Indeed, when only *distancing* strategy is applied, the robot  $E-E$  has a displacement limit since its base is fixed, while *dodging* strategy takes another direction than obstacle and does not present such an issue. Despite good results of *dodging* strategy as well, this method can present some limitations related to the *dodging* vector  $\vec{F2}$  (6) that vanishes if the vector  $\vec{d}$  is perpendicular to the plan  $(X_e, Y_e)$ , canceling thus any dodging action when it is needed the most. Furthermore, if this vector changes direction when obstacle is too close to  $E-E$  (*i.e.* high force intensity), it can induce a discontinuity on the robot applied wrench. However, it is an unlikely situation since the obstacle's

natural movement should not lead to it. The two strategies are not completely independent since in *dodging strategy* there is a weighted vector related to *distancing*. Therefore, switching between one method to another, can be smooth by adapting vectors weights. In this case, the distance and obstacle's speed should be further considered to adapt the contribution of each strategy (*distancing* or *dodging*) through their vector weights. This adaptation and its strategy should be explored in future works.

A limitation of the repulsive force model with *safety contour* appears if the safety distance can not be maintained (e.g. the obstacle's speed is higher than the maximum speed of the robot's *E-E*). In this case the direction of the force (3) still remains the same however, the intensity (4) decreases once the robot's *E-E* crosses the contour limits, while it is supposed to keep increasing. In this context, the method faces a dilemma when the robot should avoid collision with fast obstacles while the robot has a limited speed for safety. Therefore, the obstacle speed should be considered in future works to adapt online the size of safety contour, but also adapt online parameters and weights related to *distancing* or *dodging* strategies.

Once repulsive forces are calculated, other robot control strategies can be expected (torque control or position control) and are planned in future works. Current work and results present a first step for a different approach of collision avoidance, in the context of hidden robot. This work is already useful when the robot is handling an object or a tool, therefore it is the *E-E* that should avoid the collisions. However, an extension of this promising strategy to all the robot's links is planned for future work as well.

## V. CONCLUSIONS AND FUTURE WORKS

In the current work, an original approach for human-robot collision avoidance was proposed to deal with the situation of the robot being hidden by obstacles. For that, the estimation of the robot's posture in real time, based on its kinematic model and the proprioceptive data (joint angles), is merged with the Kinect 3D depth data of the environment. This allowed the obstacle-robot distance evaluation in depth space and generates a repulsive force to control the robot at the wrench level. Two main collision avoidance strategies (*distancing* and *dodging*) were implemented and tested. Results of both strategies highlighted a good collision avoidance for all tests, which is materialized by a minimum distance of about 240mm between obstacle and robot *E-E*, even when the robot is in an occluded zone (hidden by the obstacle). In future works, other robot control law and the online adaptation of parameters, vector weights and safety contour size to make a robust behavior should be addressed. The collision avoidance between dynamic obstacles and the other robot links should be explored as well.

## ACKNOWLEDGMENT

Thanks to the BRAFITEC (Brazil France Technology) program to support this research. In memory of F. Flacco, whose works inspired us for this work.

## REFERENCES

- [1] J. T. C. Tan, F. Duan, Y. Zhang, K. Watanabe, R. Kato, and T. Arai, "Human-robot collaboration in cellular manufacturing: Design and development," *2009 IEEE/RSJ International Conference on Intelligent Robots and Systems, IROS 2009*, pp. 29–34, 2009.
- [2] J. Krüger, T. K. Lien, and A. Verl, "Cooperation of human and machines in assembly lines," *CIRP Annals - Manufacturing Technology*, vol. 58, no. 2, pp. 628–646, 2009.
- [3] A. D. Santis, B. Siciliano, A. D. Luca, and A. Bicchi, "An atlas of physical human – robot interaction," *Mechanism and Machine Theory*, vol. 43, pp. 253–270, 2008.
- [4] R. Alami, A. Albu-Schaeffer, A. Bicchi, R. Bischoff, R. Chatila, A. De Luca, A. De Santis, G. Giralt, J. Guiochet, G. Hirzinger, F. Ingrand, V. Lippiello, R. Mattone, D. Powell, S. Sen, B. Siciliano, G. Tonietti, and L. Villani, "Safe and dependable physical human-robot interaction in anthropic domains: State of the art and challenges," in *2006 IEEE/RSJ International Conference on Intelligent Robots and Systems*, Oct 2006, pp. 1–16.
- [5] D. Popov, A. Klimchik, and N. Mavridis, "Collision detection, localization & classification for industrial robots with joint torque sensors," *RO-MAN 2017 - 26th IEEE International Symposium on Robot and Human Interactive Communication*, vol. 2017-Janua, no. May 2018, pp. 838–843, 2017.
- [6] A. De Luca and F. Flacco, "Integrated control for pHRI: Collision avoidance, detection, reaction and collaboration," *Proceedings of the IEEE RAS and EMBS International Conference on Biomedical Robotics and Biomechanics*, pp. 288–295, 2012.
- [7] F. Flacco, T. Kröger, A. De Luca, and O. Khatib, "A depth space approach to human-robot collision avoidance," *Proceedings - IEEE International Conference on Robotics and Automation*, pp. 338–345, 2012.
- [8] B. Schmidt and L. Wang, "Depth camera based collision avoidance via active robot control," *Journal of Manufacturing Systems*, vol. 33, no. 4, pp. 711–718, 2014. [Online]. Available: <http://dx.doi.org/10.1016/j.jmsy.2014.04.004>
- [9] J.-H. Chen and K.-T. Song, "Collision-Free Motion Planning for Human-Robot Collaborative Safety Under Cartesian Constraint," *2018 IEEE International Conference on Robotics and Automation (ICRA)*, pp. 1–7, 2018.
- [10] M. Safaea and P. Neto, "KUKA Sunrise Toolbox: Interfacing Collaborative Robots with MATLAB," *IEEE Robotics and Automation Magazine*, vol. 26, no. 1, pp. 91–96, 2019.
- [11] F. Flacco, T. Kroeger, A. De Luca, and O. Khatib, "A Depth Space Approach for Evaluating Distance to Objects: with Application to Human-Robot Collision Avoidance," *Journal of Intelligent and Robotic Systems: Theory and Applications*, vol. 80, pp. 7–22, 2015.
- [12] O. Wasenmüller and D. Stricker, "Comparison of kinect v1 and v2 depth images in terms of accuracy and precision," *Lecture Notes in Computer Science (including subseries Lecture Notes in Artificial Intelligence and Lecture Notes in Bioinformatics)*, vol. 10117 LNCS, pp. 34–45, 2017.
- [13] K. R. Group, "KUKA Sunrise.Connectivity FRI 1.7. Augsburg, Germany, 1st edition," pp. 1–59, 2015.
- [14] C. Gaz and A. De Luca, "Payload estimation based on identified coefficients of robot dynamics - With an application to collision detection," in *IEEE International Conference on Intelligent Robots and Systems*, vol. 2017-Sept, 2017, pp. 3033–3040.
- [15] W. Zhang, X. Ma, L. Cui, and Q. Chen, "3 points calibration method of part coordinates for arc welding robot," in *Intelligent Robotics and Applications*, C. Xiong, Y. Huang, Y. Xiong, and H. Liu, Eds. Berlin, Heidelberg: Springer Berlin Heidelberg, 2008, pp. 216–224.
- [16] S. Y. Chen, "Kalman filter for robot vision: A survey," *IEEE Transactions on Industrial Electronics*, vol. 59, no. 11, pp. 4409–4420, Nov 2012.
- [17] O. Khatib, "Real-time obstacle avoidance for manipulators and mobile robots," in *Proceedings. 1985 IEEE International Conference on Robotics and Automation*, vol. 2, March 1985, pp. 500–505.
- [18] A. Albu-Schäffer, S. Haddadin, C. Ott, A. Stemmer, T. Wimböck, and G. Hirzinger, "The DLR lightweight robot: Design and control concepts for robots in human environments," *Industrial Robot*, vol. 34, no. 5, pp. 376–385, 2007.